Actuator Line Method for Helicopter Rotors Computations in Various Flight Conditions

Reda Merabet * and Eric Laurendeau†
Polytechnique Montréal, Montréal, Québec, Canada

This paper presents the application of high fidelity Computational Fluid Dynamics methods for the aerodynamic evaluation of helicopter rotors in three flight conditions: hover, axial flight and placed in a confined environment. Two computational methods are considered and simulated across a range of parameter for the three flight cases. The traditional overset fully blade resolved simulation is used as a reference for the recently developed actuator line method (ALM). The latter is widely used in the wind energy sector for wind turbine simulation. The ALM replaces the explicit blade geometries by momentum source terms that re-create typical rotor flowfield characteristics in addition to providing full performance predictive capabilities. The elimination of blade meshes allows the ALM to have a lower computational cost compared to fully blade resolved simulations on the order of the mesh reduction ratio.

Nomenclature

C_d	=	Blade section 2D Drag coefficient
C_l	=	Blade section 2D Lift coefficient
$\overline{C_P}$	=	Average pressure coefficient, $\frac{\overline{p}-p_\infty}{0.5\rho_\infty V_{ind}^2}$
C_Q	=	Rotor torque coefficient, $\frac{Q}{\rho_\infty {V_{\text{tip}}}^2 A_{\text{disk}} R}$
C_T	=	Rotor thrust coefficient, $\frac{T}{\rho_\infty {V_{\text{tip}}}^2 A_{\text{disk}}}$
c	=	Local chord, m
FoM	=	Figure of merit, $\frac{{C_T}^{1.5}}{\sqrt{2}C_Q}$
M	=	Mach number
r	=	Radial coordinate along span
Re	=	Reynolds number
V_{c}	=	Climb velocity, m/s
V_{ind}^{hover}	=	Hover induced velocity, $V_{tip}\sqrt{C_T/2}$
V_{tip}	=	Velocity of the blade tip, m/s

Presented at CASI AERO 2021 – Canadian Aeronautics and Space Institute, June 14 – 18 2021, Online, Canada
*Ph.D. Candidate, Mechanical Engineering, 2900 Boulevard Édouard-Montpetit, C.P. 6079, Centre-Ville; reda.merabet@polymtl.ca
†Professor, Mechanical Engineering, 2900 Boulevard Édouard-Montpetit, C.P. 6079, Centre-Ville; eric.laurendeau@polymtl.ca

z = Rotor axial axis coordinate

σ = Rotor solidity, $\frac{N_b c_{\text{ref}}}{\pi R}$

Θ_{75} = Collective pitch at 75% blade span, degree

I. Introduction

Helicopters, due to their vertical flight capabilities, are used to access hard to reach destinations and land on complicated terrain with potentially challenging flowfield. Some of these applications are the operation of the rotor near the ground, walls or even on a ship landing platform in the possible presence of wind. Numerical simulation of such conditions can be achieved by different methods ranging in accuracy and computational time. Simpler methods such as Blade Element Momentum Theory (BEMT) [1] or singularity based methods [2–6] are computationally efficient and yield good agreement on simple cases and geometries such as an isolated rotor in hover, but are restrictive when more complex cases are considered as they would rely on extensive calibration through empiricism or complex modelling [7, 8]. On the other hand, high fidelity methods such as Unsteady Reynolds Averaged Navier Stokes (U-RANS) and other mesh based Computational Fluid Dynamics (CFD) methods [9–11] are more accurate because the equations that are solved are more complete in their formulations and the underlying physics is better captured. One hindrance of these CFD methods is that they require orders of magnitude more computational time due to the need to accurately represent the rotor geometry and their boundary layer with a large number of grid cells. To save on computational time, a growing class of methods that remove the explicit rotor geometry to replace its effect by momentum source terms while retaining the background grid is increasingly being used and developed. These methods are particularly suited for rotor-wake interaction studies where the effects of the rotor wake on the surrounding environment (fuselage, ground, obstacle) is of greater importance than precise rotor loads required for design purposes.

Different levels of modelling complexity are used for these rotor replacement techniques applied to helicopter rotors. First, the well known Actuator Disk (AD) [12, 13] typically averages azimuthally the rotor loads over the disk before projecting them onto the flowfield either as a pressure discontinuity or momentum source terms added to the flow equations. Unsteady versions of the AD also exist[14]. A further evolution is the Actuator Line Method (ALM) which considers the individual rotor blades as lines of momentum source terms that rotate in the field [15–17]. A Blade Element Theory (BET)[1] approach is typically used to evaluate the blade loading. The resulting flowfield reproduces key rotorcraft wake elements, most notably the helical tip vortex wake. Finally, the Actuator Surface Method (ASM) and Actuator Blade (AB) build on the same concept, but also feature a chordwise distribution of the blade force[18, 19].

This work presents the application of the ALM, originally introduced by Sørensen and Shen [20] for wind turbine simulations, to helicopter rotors. The method replaces the effects of the blades on the flowfield through source terms that emulate the actual blade loading in a fully predictive fashion without relying on pre-specified loading distribution or

excessive modelling. The method is capable of predicting, with a comparable accuracy to Blade Resolved (B-R) U-RANS simulations, the rotor performance coefficients, blade loading, tip vortex positions, general flowfield characteristics and surface pressure coefficient on a fuselage. The model is verified and validated on the well known S-76 rotor model in hover with comparisons made with both experimental data and Blade Resolved simulations with an extension to axial flight. Then, a rotor in ground effect, forward flight, and placed in a confined environment in the presence of a box-shaped obstacle is explored and compared to both experimental data and B-R simulations of a simplified scaled helicopter.

II. Test Cases & Rotor Geometries

Three different rotor geometries are considered as they correspond to three sets of experimental data representing different helicopter flight conditions. The chosen geometries all feature realistic rotor blade shapes and characteristics in terms of aspect ratio. However, contrary to real helicopters which usually feature articulated blades with cyclic control, the three datasets consider a rigid, un-articulated and fixed collective without cyclic pitch variation. Furthermore, as the experimental model rotors are scaled, Reynolds and Mach numbers are lower than real full scale helicopters. Even with these simplifications, the core physical phenomena are captured and well represented. The geometrical simplifications allow for better comparisons on a purely aerodynamic standpoint which is interesting in the scope of CFD code validation.

For hover, the chosen geometry is the well known S-76 rotor from the the experimental study of Balch and Lombardi [21, 22]. The geometry has been used as one of the central test case of the AIAA Hover Prediction Workshop. The rotor geometry is summarized in Table 1. Different tip geometries and Mach numbers have been studied. This work focuses on the rectangular tip at $M_{tip} = 0.6$.

Table 1 Rotor Characteristics: Hover

Rotor Definition		**Blade sections definition**			
	value	Section	Twist	Thickness	Airfoil
		(r/R)	(deg)	$(t/c$ %)	
Nb. Blades (N_b)	4	0.189	4.01	13	SC1013-R8
Rotor Radius (R)	56.04 in	0.285	4.5	10.09	Blend
Reference Chord (c_{ref})	3.1 in	0.400	3.5	9.4	SC1094-R8
Aspect Ratio (AR)	18.077	0.750	0	9.4	SC1094-R8
Solidity (σ)	0.07043	0.800	-0.5	9.4	SC1094-R8
Linear Twist	-10°	0.840	-0.9	9.5	SC1095
		0.950	-2	9.5	SC1095
		1.000	-2.5	9.5	SC1095

For axial flight, the geometry presented in Felker and McKillip [23] is considered. The rotor features relatively low

Mach and Reynolds numbers as a result of its use as a Froude scaled rotor. The rotor was tested on the unique Princeton Long Track which mounted the rotor onto a sled and moved the whole assembly in still air in order to simulate climb and descent conditions. The main geometrical features of the rotor are presented in Table 2.

Table 2 Rotor Characteristics: Axial Flight

Rotor		**Blade**	
Nb. Blades (N_b)	4	Airfoil Profile, constant	NACA0015
Rotor Radius (R)	1.2192 m	Reference Chord (c_{ref})	0.0635 m
Collective, fixed (Θ_{75})	9.3°, 10.9°	Linear Twist	-8°
Rotational Speed (Ω)	430.78 RPM	Tip Velocity (V_{tip})	55 m/s
Solidity (σ)	0.0633	Tip Mach number (M_{tip})	0.16
Aspect Ratio (AR)	19.2	Tip Reynolds number (Re_{tip})	212103

Finally, for the evaluation of a rotor operating in confined areas, the geometry presented in Zagaglia et al.[24] is used. The fuselage geometry is based on a reduced scale MD-500 helicopter whereas the rotor features four blades with a simple airfoil profile with a more complete description presented in Table 3. The rotor has been studied in the Politecnico de Milano wind tunnel where a cuboid obstacle of size 1 m x 0.45 m x 0.8 m (W x H x L) was placed. During the test campaign, different configurations were studied in terms of rotor movement sweeps, presence and localization of the obstacle. All tests were performed both in the absence of wind and with a constant wind blowing at a velocity of 5.07 m/s which corresponds to an advance ratio of $\mu = 0.05$.

Table 3 Rotor Characteristics: Confined Areas

Rotor		**Blade**	
Nb. Blades (N_b)	4	Airfoil Profile, constant	NACA0012
Rotor Radius (R)	0.375 m	Reference Chord (c_{ref})	0.032 m
Collective, fixed (Θ_{75})	10°	Linear Twist	0°
Aspect Ratio (AR)	11.72	Tip Mach number (M_{tip})	0.3
Solidity (σ)	0.10865	Tip Reynolds number (Re_{tip})	220000
Rotational Speed (Ω)	2580 RPM		

III. Numerical Modelling

Star-CCM+ 12.06 [25] is the software used in this work. It is a general purpose finite volume, unstructured, cell centred, multi-physics flow solver. All computations have been performed through schemes with 2nd order accuracy in both time and space using either the SIMPLE [26] algorithm or a density-based coupled Weiss-Smith preconditioned Roe flux-difference-splitting scheme [27] depending on the blade tip Mach number. The time marching approach uses a dual time stepping scheme with all simulations having an equal time-step equivalent to 1^o of azimuthal rotation. The U-RANS equations are closed with the $k-\omega$ SST turbulence model [28]. For fair comparison, every ALM and B-R

background meshes are of similar size and grid resolution and range from 10 to 20 million cells. In addition to the background meshes, the B-R adds individually meshed blades to the simulation through the overset method. Each individual blade is meshed with a cell count on the order of 5 to 10 million cells depending on the aspect ratio. The ALM is implemented as an external library loaded into Star-CCM+ through the User Coding framework. The library is written in C with the parallelization performed through the same MPI implementation as the base flow solver for communications.

The ALM removes the blade geometries from the computational domain and replaces their effect by momentum source terms as shown in Eqs.(1-3)

$$\frac{\partial}{\partial t}\int_V \rho\, dV + \oint_A \rho \mathbf{v} \cdot\, d\mathbf{a} = 0 \tag{1}$$

$$\frac{\partial}{\partial t}\int_V \rho \mathbf{v}\, dV + \oint_A \rho \mathbf{v} \otimes \mathbf{v} \cdot\, d\mathbf{a} + \oint_A p\mathbf{I} \cdot\, d\mathbf{a} = \oint_A \mathbf{T} \cdot\, d\mathbf{a} - \int_V \mathbf{f_{alm}}\, dV \tag{2}$$

$$\frac{\partial}{\partial t}\int_V \rho E\, dV + \oint_A \rho H \mathbf{v} \cdot\, d\mathbf{a} + \oint_A \mathbf{q} \cdot\, d\mathbf{a} = \oint_A \mathbf{T} \cdot \mathbf{v}\, d\mathbf{a} - \int_V \mathbf{f_{alm}} \cdot \mathbf{v}\, dV \tag{3}$$

In addition to the solved flow variables (the density ρ, the velocity vector $\mathbf{v}$, the pressure p, the viscous stress tensor $\mathbf{T}$, the heat flux $\mathbf{q}$, and the total energy and enthalpy E and H), there is an extra term, $\mathbf{f_{alm}}$, on the right hand side of the momentum and energy equations acting as a momentum volumetric source term and its associated work. The negative signs specify the term to be acting in equal magnitude, but opposite direction of the rotor forces thus imparting the rotor forces onto the flowfield.

To compute the $\mathbf{f_{alm}}$ term, a BET approach is taken. The rotor blades are discretized into blade segments along the quarter chord span axis. The local velocity is evaluated at these points through the integral velocity sampling [16, 29, 30] in combination with the rotational velocity yielding a effective freestream velocity $\mathbf{U_{rel}}$ and angle of attack α_{rel}. With these two values, the local lift and drag forces are evaluated from pre-computed 2D airfoil polars as per Eqs.(4) and (5).

$$\Delta L = \frac{1}{2}\rho \|\mathbf{U_{rel}}\|^2 C_l(\alpha_{\text{rel}}, \text{Re}, M) c \Delta R \tag{4}$$

$$\Delta D = \frac{1}{2}\rho \|\mathbf{U_{rel}}\|^2 C_d(\alpha_{\text{rel}}, \text{Re}, M) c \Delta R \tag{5}$$

With the locally computed lift and drag forces at every ALM control points, the solution for the complete rotor is re-constructed by summing all the force vectors multiplied by a Gaussian kernel as shown in Eqs.(6) and (7). The Gaussian kernel spreads the point force over several grid cells through the smearing parameter ϵ. This parameter is scaled with the local chord of the blade with values around $\epsilon \sim 0.25c$ producing the best results [30–33]. The source term is also radially truncated to respect the geometrical limits of the rotor blades and re-normalized in order for the

force to be completely projected into the flow domain.

$$g(x,y,z) = \frac{1}{\epsilon^3 \pi^{\frac{3}{2}}} \exp\left(-\frac{(x-x_0)^2 + (y-y_0)^2 + (z-z_0)^2}{\epsilon^2}\right) \tag{6}$$

$$\mathbf{f_{alm}} = \sum_i \cdot g_{\mathrm{i}} \cdot \left(\Delta L_i \mathbf{e_{L,i}} + \Delta D_i \mathbf{e_{D,i}}\right) \tag{7}$$

IV. Results

A. Hover

First, a collective sweep is performed to identify the the hover performance coefficients of the rotor with the results presented in Fig.1. Both the ALM and B-R solutions show excellent thrust predictive capabilities with the ALM slightly underestimating the thrust at higher collectives. The torque coefficient as a function of the thrust is slightly overestimated by the ALM which results in a lower figure of merit at a given thrust. To explain this difference, the blade thrust and torque loading at a similar trim state of $C_T/\sigma = 0.09$ is presented in Fig.2. We can observe the excellent agreement between the two methods for the first 80% blade span. Past this point, the ALM under and over predicts the thrust loading on both sides from the 92% blade span location. This is caused by the encounter of the previous blade's tip vortex causing excessive up and down-wash. This blade vortex interaction (BVI) in turn modifies the torque distribution resulting in excessive drag generation near the blade tip.

B. Axial Flight

Moving from a rotor in hover to a climbing condition, the additional freestream velocity effectively increases the inflow velocity above the rotor disk thus reducing the effective angle of attack at a given collective causing a reduction in thrust output. Furthermore, according to momentum theory, the power required for a rotor in climb corresponds to the sum of hover induced power and the climb induced power. One can therefore expect a linear trend for the figure of merit as a function of the climbing velocity [35]. Figure 3 presents the thrust coefficient and figure of merit, normalized by their respective hover values, as a function of the climb velocity V_c normalized by the hover induced velocity $V_{ind}^{hover} = V_{tip}\sqrt{C_T/2}$. The reduction in thrust is captured by both numerical methods and agree well between them along with a fair agreement with the experimental data. The linear trend in figure of merit variation is otherwise excellent. However, the two methods fail to accurately capture the proper behaviour in descent. The experimental data presented in Felker and McKillip [23] reports highly unsteady loads and the presence of vortex ring state (VRS) around the rotor. Both simulations at $V_c/V_{ind}^{hover} = -0.75$ still show near-steady converged thrust signals with no apparent presence of VRS around the rotor. However, the far-wake shows some asymmetry which might be indicative of VRS onset.

Figure 4 presents the locations of the tip vortices for the two methods in different axial flight conditions. First, in

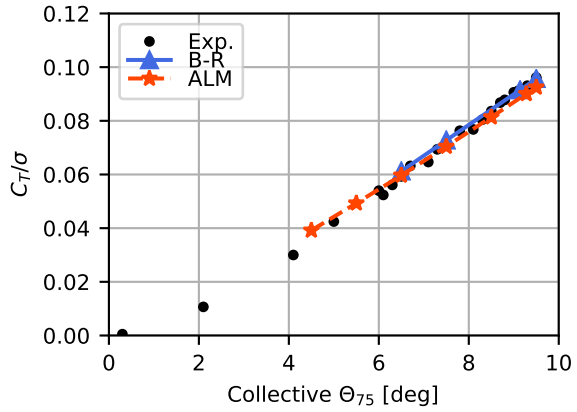

(a) Thrust Coefficient

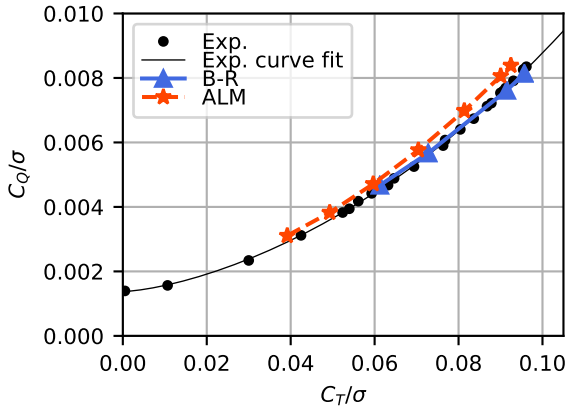

(b) Torque Coefficient

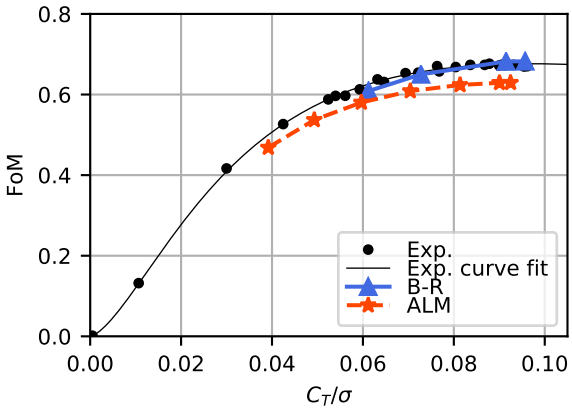

(c) Figure of Merit

Fig. 1 Integrated rotor performance coefficients for the ALM and B-R in hover adapted from [34]

hover, the two methods are in excellent agreement between each other and with the empirical prescribed wake model of Kocurek and Tangler [36]. Although there is a slight lag in the axial velocity between the second and fifth blade passage. In climb at $V_c/V_{ind}^{hover} = 0.75$, the added downward velocity advects the tip vortices faster than in hover despite the loss of thrust (and therefore loss of hover induced velocity). The radial contraction is also considerably reduced. The two numerical methods are nearly indistinguishable from each other. Finally, in descent at $V_c/V_{ind}^{hover} = -0.25$, the wake is less stable resulting in a tip vortex extraction stopped after four blade passages only. As intuition might suggest, the trend is opposite to the climbing case with the wake contracting more than in hover along with a slower axial advection.

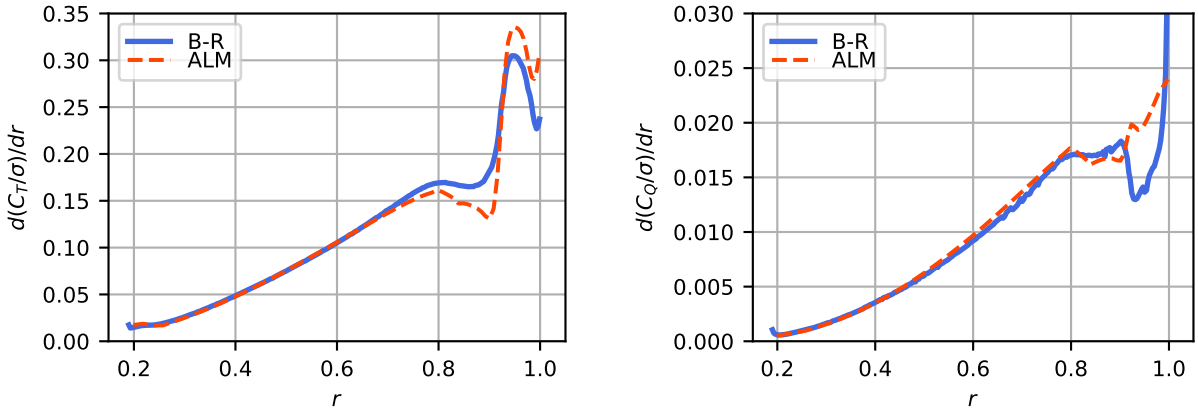

(a) Thrust Loading **(b) Torque Loading**

Fig. 2 Sectional blade loading at $C_T/\sigma = 0.09$ in hover adapted from [34]

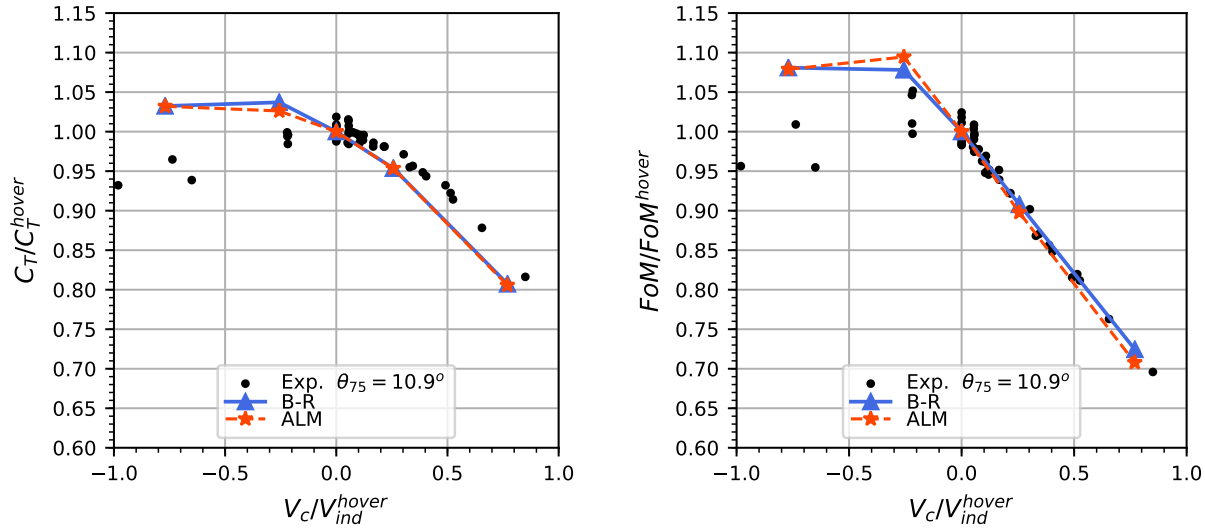

(a) Thrust Coefficient **(b) Figure of Merit**

Fig. 3 Integrated rotor performance coefficients for the ALM and B-R in axial flight

C. In Confined Areas

To evaluate a rotor in confined areas (where the rotor sees at least one of its movement restricted by a geometry), two configurations from the dataset of Zagaglia et al. [24] are considered. The first considers the classic case of hover in ground effect with the rotor placed above a ground plane with a varying vertical height. The second adds a cuboid obstacle $2R$ away from the rotor that is still placed at various height above the ground. Figure 5 presents the thrust ratios normalized by the out-of-ground effect (OGE, $Z/R = 4.0$) thrust value for both the considered cases. For the ground only case, a reference empirical relation of Cheeseman and Bennett [37] is added for comparison purposes.

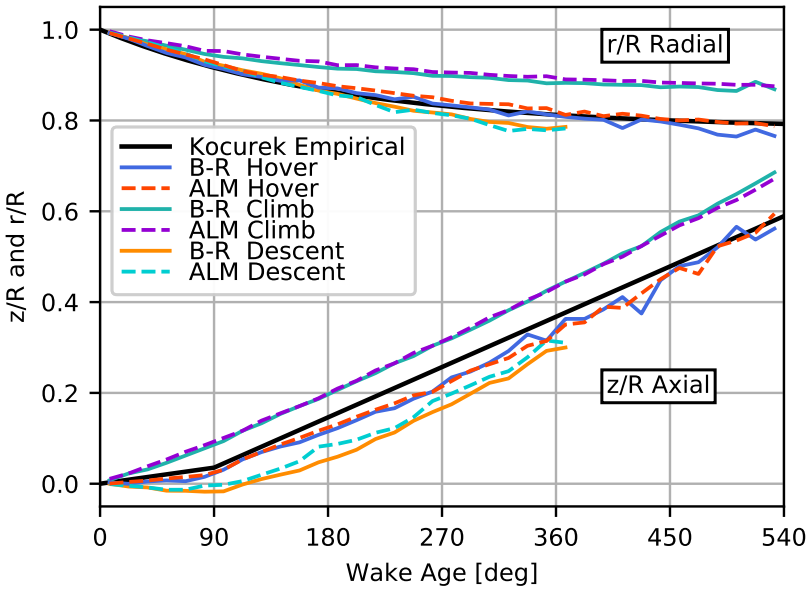

Fig. 4 Tip vortex positions at for the ALM and B-R in axial flight at fixed collective $\Theta_{75} = 10.9^o$

Both the ALM and B-R are in excellent agreement between them and predict the observed thrust augmentation at a fixed collective when the rotor is moved closer to the ground. The effect on the flowfield is illustrated in Fig.6 where we can see the wake of the ALM changing from the typical contraction observed in hover towards an expansion due to ground effect. Notice the higher up-wash present at the centre of the rotor past the blade root.

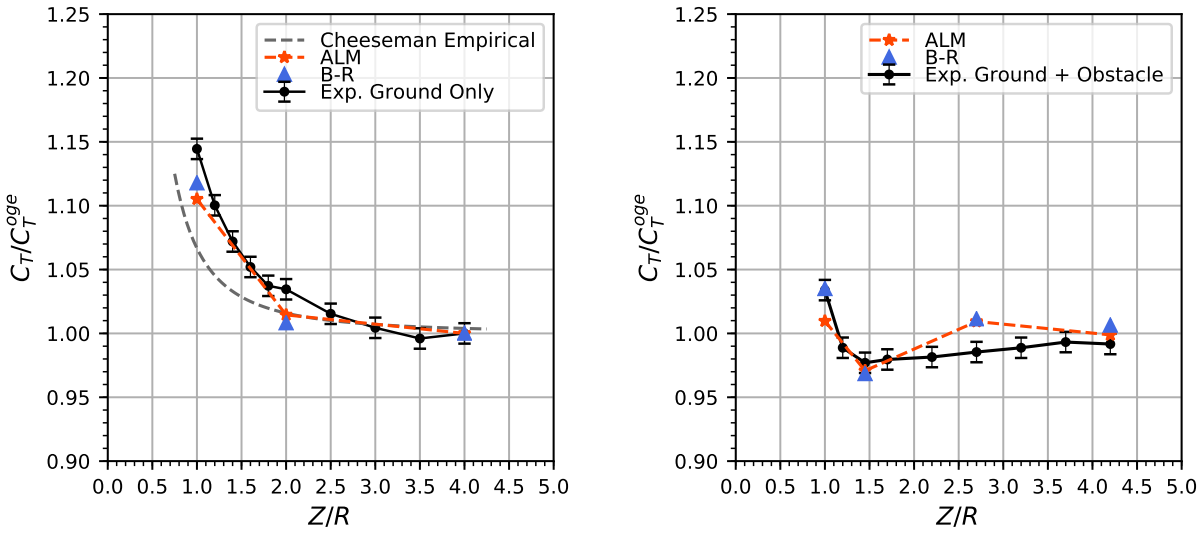

(a) Ground only **(b) Ground + obstacle**

Fig. 5 Rotor in confined areas - Thrust coefficient ratio comparison adapted from [38]

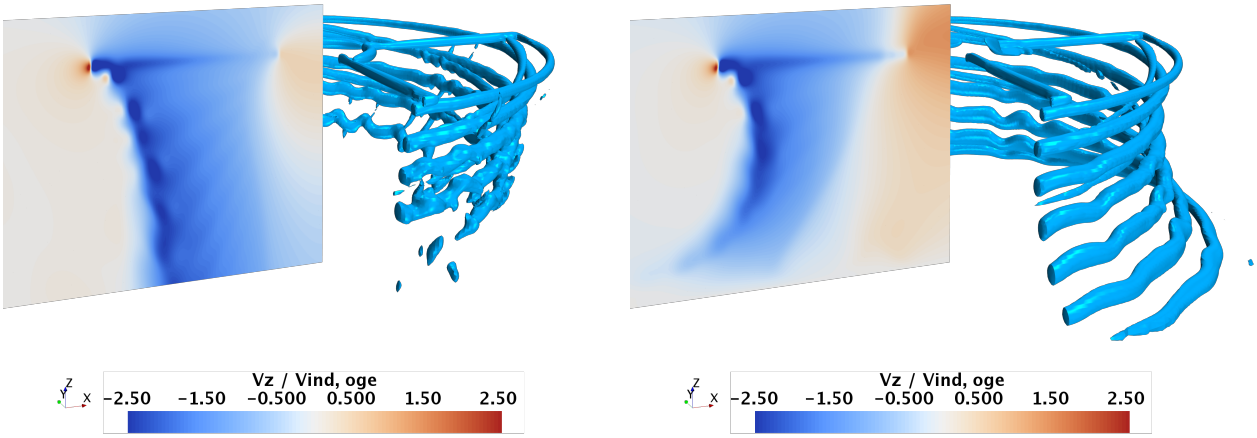

(a) ALM hover $Z/R = 4$ **(b) ALM hover** $Z/R = 1$

Fig. 6 Instantaneous axial velocity and Q-criterion contour for the ALM in ground effect adapted from [38]

Adding the obstacle yields a considerable reduction in the thrust rise compared to the ground only case. Again, the two numerical methods are in good agreement with each other whereas the experimental data agreement is observed at the two ends of the vertical sweep. At $Z/R = 2.7$, both methods overestimate the thrust. This is explained by the lengthiness of wake development of this particular case and the excessive computational resources to achieve a sufficient simulation time. With the obstacle, the wake has a tendency to stream downwards below the rotor, re-orient itself hitting the ground and then again stream upwards upon meeting the obstacle vertical wall. This essentially creates a re-circulation zone between the rotor and the obstacle. At lower heights, the rotor re-ingest its own recirculated wake resulting in higher inflow and therefore reducing the blade effective angle of attack and therefore the thrust. Further away from the ground, the rotor is less affected by the re-circulation effect. Rotor at mid-heights are somewhat affected, but the re-circulation pattern takes a long time to establish itself which results in excessively lengthy simulation times. The re-circulation patterns can be observed in Fig.7.

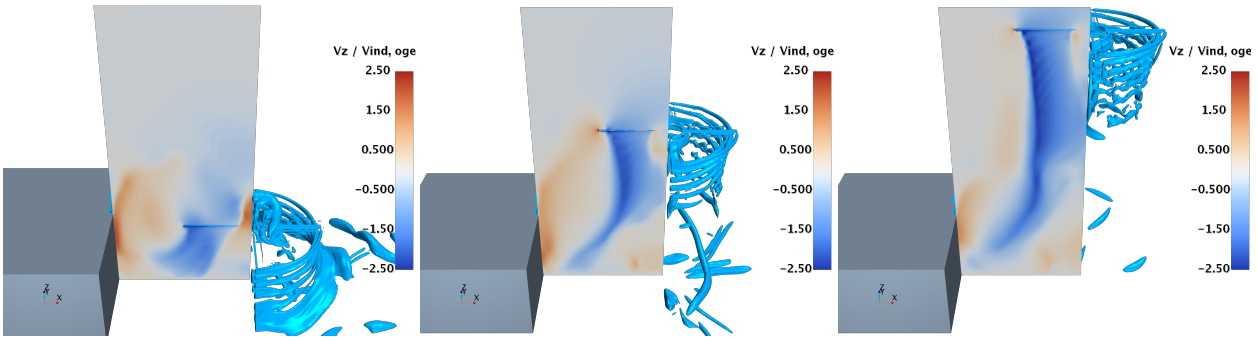

(a) B-R $Z/R = 1.00$ **(b) B-R** $Z/R = 2.70$ **(c) B-R** $Z/R = 4.20$

Fig. 7 Instantaneous axial velocity and Q-criterion contour for the B-R in ground+obstacle effect from [38]

Finally, as a showcase of additional capabilities, the rotor with its fuselage are placed in forward flight. Figure 8 relates the average pressure coefficient over the fuselage for both the ALM and blade resolved simulations. The two methods present near identical average pressure distribution alongside a similar tip vortex wake pattern.

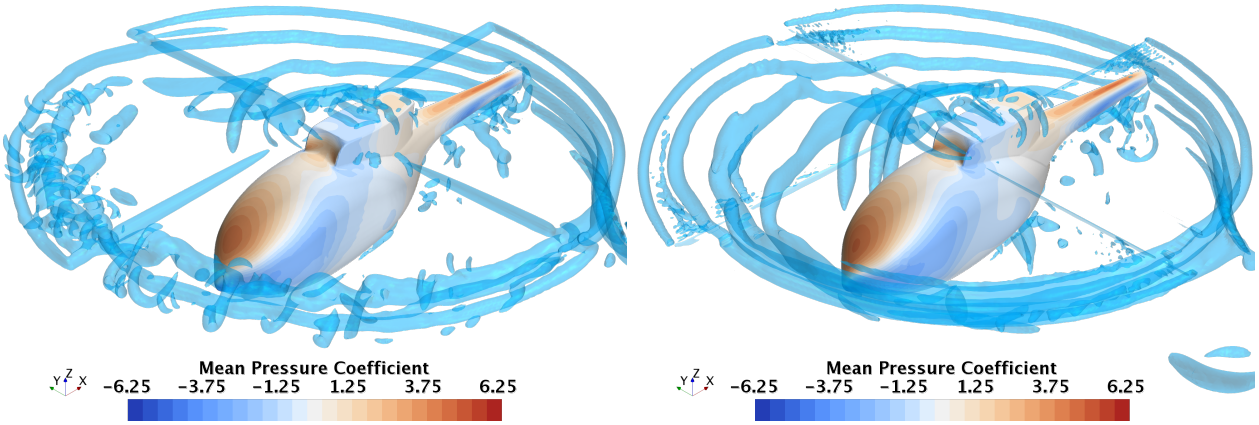

(a) ALM forward flight - $\mu = 0.05$**,** $Z/R = 4$ **(b) B-R forward flight -** $\mu = 0.05$**,** $Z/R = 4$

Fig. 8 Average surface pressure coefficient and Q-criterion contour adapted from [38]

D. Computational Time Comparison

The end goal of developing a rotor replacement technique, namely the actuator line method in this case, is to save on computational time when compared to traditional blade resolved simulations through mesh reduction. Table 4 presents the total mesh count and ratio for the three selected test cases in addition to the computational time and associated speed-up. As expected, the ALM has a computational speed-up proportional to its mesh reduction ratio. In fact, the speed-up is greater than the mesh ratio as a result of the superior parallel efficiency of the ALM when compared to the B-R case that relies on the overset technique significantly hindering parallel performances. As a an assessment of the limited overset scaling capabilities, the computational time per revolution results presented in Table 4 for the B-R Axial Flight case have been run on 480 CPU cores. The same mesh running on 1000 cores would have a CPU time per revolution of 3758 hrs, a clear loss in parallel efficiency due to poor scaling. The ALM on the other hand would produce a better scaling past 1000 cores on its given mesh. Therefore, ALM is not only faster due to lesser mesh sizes, but also allows a greater scalability and the opportunity to run full helicopter CFD simulations in order of hours/days, given sufficient compute resources. By opposition, overset blade resolved simulations are typically constrained to run over several days or weeks as they are curtailed to run on lower core counts in order to satisfy some minimum computational efficiency target to minimize compute time allocation waste. Furthermore, the ALM is mush less sensible to mesh coarsening than B-R solutions which can further increase the total computational speed-up the method provides.

Table 4 Compute time averaged for one revolution and Speed-up

	Mesh Size [Millions]		
	Hover	Axial Flight	Confined Areas
B-R	28.7	47.1	32.9
ALM	10.1	20.4	18.0
Ratio	2.84	2.31	1.83
	CPU time per revolution [hr]		
	Hover	Axial Flight	Confined Areas
B-R	2321.5	2504	1661.2
ALM	741.9	880.0	824.3
Speed-up	3.1	2.84	2.02

V. Conclusions

This paper presented the application of two high fidelity CFD based simulation tools towards helicopter rotors placed in various flight conditions. The developed rotor replacement technique, the actuator line method, showed excellent consistency and trend predictive capabilities when compared to the more traditional overset blade resolved simulations. The two methods also show good agreement with reference experimental data. However, one drawback of the ALM compared to an equivalent B-R simulation is the handling of perpendicular BVI that cause blade thrust loading over and under-prediction ultimately resulting in a slightly higher torque. Otherwise, for the remaining of the presented metrics, the ALM showed results on par with B-R solutions with a substantial economy in computational time. This economy comes from a lower mesh cell count as well as higher parallelization capabilities.

VI. Acknowledgments

This work was funded by CAE Inc. and the Natural Sciences and Engineering Research Council (NSERC) of Canada. This research was enabled in part by support provided by Calcul Quebec and Compute Canada for the compute resources.

References

[1] Johnson, W., Helicopter Theory, Dover Publications, New York, 1994.

[2] Quackenbush, R., Chua, K., Wachspress, D. A., and Boschitsch, H., "Computation of Rotor Aerodynamic Loads in Forward Flight Using a Full-Span Free Wake Analysis," NASA CR 177611, NASA, Oct. 1990.

[3] Ferlisi, C., "Rotor Wake Modelling Using the Vortex-Lattice Method," Master's thesis, Ecole Polytechnique Montreal, Montreal, Canada, Apr. 2018.

[4] Katz, J., and Plotkin, A., Low-Speed Aerodynamics, 2nd ed., Cambridge University Press, New York, 2001.

[5] Griffiths, D. A., Ananthan, S., and Leishman, J. G., "Predictions of Rotor Performance in Ground Effect Using a Free-Vortex Wake Model," Journal of the American Helicopter Society, Vol. 50, No. 4, 2005, pp. 302–314. https://doi.org/10.4050/1.3092867.

[6] Gallas, Q., Boisard, R., Monnier, J.-C., Pruvost, J., and Gilliot, A., "Experimental and numerical investigation of the aerodynamic interactions between a hovering helicopter and surrounding obstacles," Milan, Italy, 2017, pp. 1–6.

[7] Tan, J. F., Zhou, T. Y., Sun, Y. M., and Barakos, G. N., "Numerical investigation of the aerodynamic interaction between a tiltrotor and a tandem rotor during shipboard operations," Aerospace Science and Technology, Vol. 87, 2019, pp. 62–72. https://doi.org/10.1016/j.ast.2019.02.005.

[8] Caprace, D.-G., Chatelain, P., and Winckelmans, G., "Wakes of rotorcraft in advancing flight: A large-eddy simulation study," Physics of Fluids, Vol. 32, No. 8, 2020, p. 087107. https://doi.org/10.1063/5.0015162.

[9] Crozon, C., Steijl, R., and Barakos, G. N., "Numerical Study of Helicopter Rotors in a Ship Airwake," Journal of Aircraft, Vol. 51, No. 6, 2014, pp. 1813–1832. https://doi.org/10.2514/1.C032535.

[10] Kalra, T. S., Lakshminarayan, V. K., and Baeder, J. D., "CFD validation of micro hovering rotor in ground effect," AHS International, Phoenix, Arizona, 2010, pp. 1–22.

[11] Brown, R. E., and Whitehouse, G. R., "Modelling Rotor Wakes in Ground Effect," Journal of the American Helicopter Society, Vol. 49, No. 3, 2004, pp. 238–249. https://doi.org/10.4050/JAHS.49.238.

[12] Rajagopalan, R. G., and Mathur, S. R., "Three Dimensional Analysis of a Rotor in Forward Flight," Journal of the American Helicopter Society, Vol. 38, No. 3, 1993, pp. 14–25. https://doi.org/10.4050/JAHS.38.14.

[13] Le Chuiton, F., "Actuator disc modelling for helicopter rotors," Aerospace Science and Technology, Vol. 8, No. 4, 2004, pp. 285–297. https://doi.org/10.1016/j.ast.2003.10.004.

[14] Boyd Jr, D. D., "Rotor/fuselage unsteady interactional aerodynamics: a new computational model," PhD Thesis, Virginia Tech, 1999.

[15] Alpman, E., Long, L. N., Bridges, D. O., and Horn, J. F., "Fully-Coupled Simulations of the Rotorcraft / Ship Dynamic Interface," American Helicopter Society International 63rd Annual Forum, AHS International, Virginia Beach, Virginia, 2007, pp. 1367–1382.

[16] Forsythe, J. R., Lynch, E., Polsky, S., and Spalart, P., "Coupled Flight Simulator and CFD Calculations of Ship Airwake using Kestrel," 53rd AIAA Aerospace Sciences Meeting, American Institute of Aeronautics and Astronautics, 2015. https://doi.org/10.2514/6.2015-0556.

[17] Delorme, Y., Stanly, R., Frankel, S. H., and Greenblatt, D., "Application of Actuator Line Model for Large Eddy Simulation of Rotor Noise Control," Aerospace Science and Technology, Vol. 108, 2021, p. 106405. https://doi.org/10.1016/j.ast.2020.106405.

[18] Linton, D., Widjaja, R., and Thornber, B., "Validation of an Actuator Surface Model with CFD-convected Wake Model for Hover and Forward Flight," Jeju Island, Korea, 2018, pp. 1–8.

[19] Kim, T., Oh, S., and Yee, K., "Novel Actuator Surface Method for Helicopter Rotor Analysis," Journal of Aircraft, Vol. 53, No. 6, 2016, pp. 1947–1952. https://doi.org/10.2514/1.C033666.

[20] Sørensen, J. N., and Shen, W. Z., "Numerical Modeling of Wind Turbine Wakes," Journal of Fluids Engineering, Vol. 124, No. 2, 2002, pp. 393–399. https://doi.org/10.1115/1.1471361.

[21] Balch, D. T., and Lombardi, J., "Experimental Study Of Main Rotor Tip Geometry And Tail Rotor Interactions in Hover Vol 1 - Text and Figures," NASA CR 177336, National Aeronautics And Space Administration, 1985.

[22] Balch, D. T., and Lombardi, J., "Experimental Study Of Main Rotor Tip Geometry And Tail Rotor Interactions in Hover Vol 2 - Run Log and Tabulated Data," NASA CR 177336, National Aeronautics And Space Administration, 1985.

[23] Felker, F. F., and McKillip, R. M., "Comparisons of Predicted and Measured Rotor Performance in Vertical Climb and Descent," American Helicopter Society 50th Annual Forum, AHS International, Washington D.C. USA, 1994.

[24] Zagaglia, D., Zanotti, A., and Gibertini, G., "Analysis of the loads acting on the rotor of a helicopter model close to an obstacle in moderate windy conditions," Aerospace Science and Technology, Vol. 78, 2018, pp. 580–592. https://doi.org/10.1016/j.ast.2018.05.019.

[25] "STAR-CCM+ Documentation," User Manual Version 12.06, Siemens PLM Software, 2016.

[26] Ferziger, J. H., and Perić, M., Computational methods for fluid dynamics, 3rd ed., Springer, Berlin ; New York, 2002.

[27] Weiss, J. M., Maruszewski, J. P., and Smith, W. A., "Implicit Solution of Preconditioned Navier-Stokes Equations Using Algebraic Multigrid," AIAA Journal, Vol. 37, No. 1, 1999, pp. 29–36. https://doi.org/10.2514/2.689.

[28] Menter, F. R., "Two-equation eddy-viscosity turbulence models for engineering applications," AIAA Journal, Vol. 32, No. 8, 1994, pp. 269–289. https://doi.org/10.2514/3.12149.

[29] Churchfield, M. J., Schreck, S. J., Martinez, L. A., Meneveau, C., and Spalart, P. R., "An Advanced Actuator Line Method for Wind Energy Applications and Beyond," 35th Wind Energy Symposium, American Institute of Aeronautics and Astronautics, 2017. https://doi.org/10.2514/6.2017-1998.

[30] Merabet, R., and Laurendeau, E., "Parametric Study on the Velocity Sampling Techniques for the Actuator Line Method in 2D," AIAA SciTech 2019 Forum, American Institute of Aeronautics and Astronautics, San Diego, California, 2019. https://doi.org/10.2514/6.2019-1797.

[31] Martinez-Tossas, L. A., Churchfield, M. J., and Meneveau, C., "Optimal smoothing length scale for actuator line models of wind turbine blades based on Gaussian body force distribution," Wind Energy, Vol. 20, No. 6, 2017, pp. 1083–1096. https://doi.org/10.1002/we.2081.

[32] Shives, M., and Crawford, C., "Mesh and load distribution requirements for actuator line CFD simulations," Wind Energy, Vol. 16, No. 8, 2012, pp. 1183–1196. https://doi.org/10.1002/we.1546.

[33] Martinez-Tossas, L. A., and Meneveau, C., "Filtered lifting line theory and application to the actuator line model," Journal of Fluid Mechanics, Vol. 863, 2019, pp. 269–292. https://doi.org/10.1017/jfm.2018.994.

[34] Merabet, R., and Laurendeau, E., "Hovering Helicopter Rotors Modeling Using the Actuator Line Method," Under Review by Journal of Aircraft, 2021.

[35] Caradonna, F., "Performance Measurement and Wake Characteristics of a Model Rotor in Axial Flight," Journal of the American Helicopter Society, Vol. 44, No. 2, 1999, pp. 101–108. https://doi.org/10.4050/JAHS.44.101.

[36] Kocurek, J. D., and Tangler, J. L., "A Prescribed Wake Lifting Surface Hover Performance Analysis," Journal of the American Helicopter Society, Vol. 22, No. 1, 1977, pp. 24–35. https://doi.org/10.4050/JAHS.22.24.

[37] Cheeseman, I. C., and Bennett, W. E., "The Effect of the Ground on a Helicopter Rotor in Forward Flight," A.R.C. Technical Report 3021, Aeronautical Research Council, London UK, Sep. 1955.

[38] Merabet, R., and Laurendeau, E., "Numerical simulations of a rotor in confined areasincluding the presence of wind," Submitted to Aerospace Science and Technology, 2021.